

BUOYANCY DRIVEN, MULTI-PHASE FLOW SIMULATIONS USING SMOOTHED PARTICLE HYDRODYNAMICS

Kamil Szewc^{1,2,3}, Jacek Pozorski¹

¹*IMP, Polish Academy of Sciences, Gdańsk, Poland;*

²*Université de Lorraine, UMR 7563, Vandoeuvre-lès-Nancy, France;*

³*CNRS, LEMTA, UMR 7563, Vandoeuvre-lès-Nancy, France;*

E-mail: kszewc@imp.gda.pl

Abstract

Smoothed Particle Hydrodynamics (SPH) is a fully Lagrangian, particle-based approach for fluid flows simulations. Its main advantage over Eulerian techniques is no need of the numerical grid. Therefore, there is no necessity to handle the interface shape. The SPH approach is suitable to use for complex geometries, multi-phase flows with interfaces or free-surface flows. In the present work we discuss the usefulness of the SPH approach for modeling multi-phase flows, governed by buoyancy. The study is supported by two- and three-dimensional cases including: the Rayleigh-Taylor & Rayleigh-Bernard instabilities, an air bubble rising in water, and also two cases not governed by buoyancy: a heat conduction in slab and the cube-to-sphere droplet deformation. The last part of the article is devoted to discussions on the potential use of SPH method to simulate phase change phenomena. The first attempts to simulate the boiling process are also described.

Key words: lagrangian approach, SPH, multi-phase flow, buoyancy force

INTRODUCTION

Smoothed Particle Hydrodynamics (SPH) is a fully Lagrangian, particle-based approach for fluid-flows simulations. This method was independently proposed by Gingold & Monaghan (Gingold et al., 1977) and Lucy (Lucy, 1977) to simulate some astrophysical phenomena at the hydrodynamic level. Nowadays, SPH is more and more often used for flows in hydroengineering (Lee et al., 2010) and in geophysical applications (Prakash et al., 2011). Its main advantage over Eulerian techniques is no need of the numerical grid. Therefore, there is no necessity to handle the interface shape, unlike it has to be done in Volume-of-Fluid, Level-Set or Front-Tracking methods. Thus, this approach is suitable to use for complex geometries, multi-phase flows with interfaces or free-surface flows. In SPH, the fluid dynamics is represented by particle evolution equations introduced through integral interpolants of field quantities.

Buoyancy driven, multi-phase flows are very common in many scientific and technical issues as nuclear reactor systems or foundry devices. In many cases, simulations of the interface position are crucial for properly modeling such processes. One of the examples is boiling process where the liquid-vapour interface location and interfacial area have a significant influence on the mass transfer. Due to this complexity, most recently developed Eulerian methods still face difficulties in a full description of boiling phenomena, involving the nucleation, growth, and detachment of vapor bubbles and possibly also transition into different boiling regimes with increasing heat flux through the wall.

In the present work we discuss the usefulness of the SPH approach for modeling multi-phase flows and its potential to simulate boiling phenomena. The study is supported by two- and three-dimensional cases involving: the Rayleigh-Taylor & Rayleigh-Bernard instabilities, and an air bubble rising in water. Two important additional validation cases, which are not governed by buoyancy, are also presented: heat conduction in a slab (validation of the energy eq. in SPH) and the cube-to-sphere deformation (surface tension validation). To properly model flows with large density differences, multi-phase SPH formulation has been used (Hu and Adams, 2006). For modeling the surface-tension phenomena, the Continuum Surface Force (Morris, 2000) technique is used. The natural convection phenomena are modeled using the Boussinesq approximation. In the work we consider both incompressible (liquid) and compressible (air in bubbles) flow regimes. This constraint is assured using weakly compressible technique, where the standard set of governing equations is closed by a suitably-chosen, artificial equation of state. In the first part of the article, the SPH method is briefly recalled. Further part of the paper contains the numerical tests. The last Section is a discussion on the usefulness of SPH for the phase transition problem with a particular focus on the boiling phenomena.

The paper offers a review of the experience of the authors with the SPH method (Szewc et al., 2011, 2012a,b), reports on their current work and provides some perspectives for next-term development of the approach (simulation of boiling regimes).

SPH FORMULATION

Basic ideas

The main idea of the SPH approach is to introduce kernel interpolants for flow quantities so that fluid dynamics is represented by a set of particle evolution equations, cf. (Monaghan, 1992) for a review. Then, three approximations are made to obtain practical formulations.

The first one is an interpolation of field quantities at a point. To construct it, we utilize an integral interpolant $\widehat{A}(\mathbf{r})$ of any field $A(\mathbf{r})$ (for simplicity we consider here a scalar field only)

$$\widehat{A}(\mathbf{r}) = \int_{\Omega} A(\mathbf{r}') W(\mathbf{r} - \mathbf{r}', h) d\mathbf{r}', \quad (1)$$

where the integration is over all the domain Ω and $W(\mathbf{r}, h)$ is a weighting function (the kernel) with the parameter h called the smoothing length. Generally, as a numerical representation of the Dirac-delta distribution, the kernel should possess a symmetrical form and, also, should be normalized. Taking into consideration computational effort and proper implementation of the boundary conditions, it is worth using kernels having a compact support. Since there are many possibilities for the choice of $W(\mathbf{r}, h)$ in order to avoid kernel artifacts such as particle clustering (Sweple et al., 1995), we use the Wendland kernel (Wendland, 1995) in the form (in 3-D)

$$W(\mathbf{r}, h) = \frac{21}{16\pi h^3} \begin{cases} \left(1 - \frac{q}{2}\right)^4 (2q + 1), & \text{for } q < 2, \\ 0, & \text{otherwise,} \end{cases} \quad (2)$$

where $q = |\mathbf{r}|/h$. An optimal choice of the kernel and of the simulation parameters has amply been discussed in Szewc et al. (2012a).

The second approximation of the SPH technique is the discretization of space. It is achieved by dividing the domain into a fine-grained representation (particles), where each particle carries the properties of the field. Then, the integral interpolant $\widehat{(\cdot)}$, Eq. (1), becomes a summation interpolant $\langle \cdot \rangle$

$$\langle A \rangle(\mathbf{r}) = \sum_b A(\mathbf{r}_b) W(\mathbf{r} - \mathbf{r}_b, h) \Omega_b, \quad (3)$$

where \mathbf{r}_b and Ω_b denote the position and volume of the particle b . Specifically, the SPH task involves the computation of the interpolant at each particle, so that Eq. (3) may be rewritten into the form

$$\langle A \rangle_a = \sum_b A_b W_{ab}(h) \Omega_b, \quad (4)$$

where $\langle A \rangle_a = \langle A \rangle(\mathbf{r}_a)$, $A_a = A(\mathbf{r}_a)$ and $W_{ab}(h) = W(\mathbf{r}_b - \mathbf{r}_a, h)$. An additional advantage of SPH is revealed when differentiation of fields is considered. In accordance with (1), the gradient of $A(\mathbf{r})$ has the form

$$\widehat{\nabla A}(\mathbf{r}) = \int_{\Omega} \nabla A(\mathbf{r}') W(\mathbf{r} - \mathbf{r}', h) d\mathbf{r}'. \quad (5)$$

Taking advantage of the integration by parts and utilizing the kernel symmetry, after discretization, the above expression can be further transformed to

$$\langle \nabla A \rangle_a = \sum_b A_b \nabla_a W_{ab}(h) \Omega_b. \quad (6)$$

Since the nabla operator acts only on the kernel, the gradient of the field is dependent only on the values of the field at particles. Higher derivatives are obtained in a straightforward manner. However, due to accuracy and efficiency requirements, the commonly used form is built as a combination of the finite difference approach and the SPH approximation (Cleary and Monaghan, 1999), cf. (16).

The third SPH approximation consists in assuming that the field value A_a at a point and its SPH approximation $\langle A \rangle_a$ are equal:

$$\langle A \rangle_a \approx A_a, \quad (7)$$

which means that the effects of scales which are typically smaller than h are smoothed out.

Governing equations

The full set of governing equations for incompressible viscous flows is composed of the Navier-Stokes (N-S) equation

$$\frac{d\mathbf{u}}{dt} = -\frac{1}{\varrho} \nabla p + \nu \nabla^2 \mathbf{u} + \mathbf{g}, \quad (8)$$

where ϱ is the (constant) density, \mathbf{u} the velocity, t the time, p the pressure, ν the kinematic viscosity and \mathbf{g} acceleration of gravitation, and the continuity equation

$$\frac{d\varrho}{dt} = -\varrho \nabla \cdot \mathbf{u} \quad (9)$$

that, in the incompressible regime, has the form of a divergence-free condition $\nabla \cdot \mathbf{u} = 0$. Since SPH is fully Lagrangian, we extend the above system by the particle advection equation

$$\frac{d\mathbf{r}}{dt} = \mathbf{u}. \quad (10)$$

Continuity equation

Using relation (6), the SPH formulation of the continuity equation (9) can be expressed in the following form

$$\frac{d\varrho_a}{dt} = \varrho_a \sum_b \mathbf{u}_{ab} \cdot \nabla_a W_{ab}(h) \Omega_b. \quad (11)$$

It is important to note that various ways to express divergence exist. Eq. (11) has been proposed by Colagrossi and Landrini (2003) to solve the problem with the instabilities occurring on the interface. However, since the form (11) does not conserve the total mass of particles explicitly, it has been decided to use an alternative approach that avoids this weakness. Based on the definition of the particle mass

$$m_a = \Omega_a \varrho_a, \quad (12)$$

the standard summation formula (4) may be used to yield

$$\varrho_a = \sum_b m_b W_{ab}(h). \quad (13)$$

The main disadvantage of this formulation is the problem of representing sharp density discontinuities at material interfaces. To avoid this difficulty, we use the proposal of Hu and Adams (2006)

$$\varrho_a = m_a \sum_b W_{ab}(h) = \frac{m_a}{\Omega_a}, \quad (14)$$

where all m_a are chosen as equal (separately for each phase). In this approach, the density field is represented only by spatial distribution of neighboring particles, but not their masses. Therefore, in multi-phase flows, particles located near an interface but belonging to different fluids may interact without having their density affected by the other fluid.

Momentum equation

The right-hand side of the Navier-Stokes equation (8) contains the contributions of pressure, viscous, surface tension and external forces. To construct an SPH method that deals properly with multi-phase flows and simultaneously assures mass conservation, Hu and Adams (2006) proposed a multi-phase formalism that can treat density discontinuities and conserves mass explicitly. In this approach, the $\varrho = \text{const}$ condition is identified with $\Omega = \text{const}$ and no SPH approximation depends explicitly on density field. In this formulation, the N-S pressure term becomes

$$\left\langle \frac{\nabla p}{\varrho} \right\rangle_a = \frac{1}{m_a} \sum_b \left(\frac{p_a}{\Omega_a^2} + \frac{p_b}{\Omega_b^2} \right) \nabla_a W_{ab}(h), \quad (15)$$

while the viscous term has the form

$$\langle \nu \nabla^2 \mathbf{u} \rangle = \frac{1}{m_a} \sum_b \frac{2\mu_a \mu_b}{\mu_a + \mu_b} \left(\frac{1}{\Omega_a^2} + \frac{1}{\Omega_b^2} \right) \frac{\mathbf{r}_{ab} \cdot \nabla_a W_{ab}(h)}{r_{ab}^2 + \eta^2} \mathbf{u}_{ab}, \quad (16)$$

where μ is the dynamical viscosity and $\eta = 0.01h$ is a small regularizing parameter. To include the hydrostatic force, the hydrostatic pressure is computed on a regular mesh and later projected on the particles (Szewc et al., 2011).

Heat transfer

Simulations of heat transfer are very important in many industrial, geophysical and astrophysical problems. In most of real (not numerical) cases, the geometry of the flow is complicated and materials are not homogeneous. Due to these inconveniences, the Lagrangian framework of Smoothed Particle Hydrodynamics can offer an advantage over Eulerian methods. Here, a short introduction to the SPH implementation of heat transfer phenomena is presented. An extensive discussion about the natural convection phenomena with a particular emphasis on the usefulness of the Boussinesq approximation is presented in (Szewc et al., 2011).

Assuming that the fluid is incompressible, the heat production due to viscous dissipation is negligible, and finally that there is no external source of energy, the equation for internal energy e evolution can be written in the form

$$\rho \frac{de}{dt} = \nabla \cdot (k \nabla T), \quad (17)$$

where T is temperature and k is conductivity. To rewrite it in terms of the temperature, it is natural to use the relation defining the specific heat c_v ($de = c_v dT$)

$$\rho c_v \frac{dT}{dt} = \nabla \cdot (k \nabla T). \quad (18)$$

After Cleary and Monaghan (1999), the simplified energy equation, Eq. (18), in the SPH form may be expressed as

$$\frac{dT_a}{dt} = \frac{4}{\rho_a c_{pa}} \sum_b \frac{k_a k_b}{k_a + k_b} \frac{T_{ab} \mathbf{r}_{ab}}{r_{ab}^2 + \eta^2} \cdot \nabla_a W_{ab}(h) \Omega_b, \quad (19)$$

where $T_{ab} = T_a - T_b$.

Surface tension

There are several ways to numerically model surface-tension effects. The most common model, introduced by Brackbill et al. (1992), is the Continuum Surface Force method (CSF) where the surface forces are interpreted as a continuous interface effects. In this approach, surface tension is simulated by computing the local curvature of the interface. However, this approach does not guarantee the exact conservation of momentum. In another variant of the CSF method, the surface

tension force per unit volume is expressed as the divergence of the capillary pressure tensor. This variant was proposed by Lafaurie et al. (1994), introduced in a SPH formulation by Morris (2000) and later improved by Hu and Adams (2006). This method is momentum conserving and the computation of local curvature is avoided but, in our validation cases (not presented in this paper), this variant has sporadically revealed itself as being unstable.

Taking into account the advantages and drawbacks discussed above, we have decided to use the CSF approach based on the computation of the local curvature in the present work. In this method, the surface tension force is converted into the force per unit volume

$$\mathbf{F}_s = \mathbf{f}_s \delta_s, \quad (20)$$

where δ_s is a suitably-chosen surface delta function and

$$\mathbf{f}_s = \sigma \kappa \widehat{\mathbf{n}} + \nabla_s \sigma, \quad (21)$$

where \mathbf{f}_s is the force per unit area, κ is the local curvature of the interface and $\widehat{\mathbf{n}}$ is the unit vector normal to the interface. The second r.h.s. term in Eq. (21), linked with the Marangoni effect, is neglected in the present work. The normal unit vectors $\widehat{\mathbf{n}}$ can be calculated using the so-called color function c

$$c_a = \begin{cases} 1, & \text{if particle } a \text{ belongs to phase 1,} \\ 0, & \text{if particle } a \text{ belongs to phase 2,} \end{cases} \quad (22)$$

using the formula

$$\widehat{\mathbf{n}} = \frac{\mathbf{n}}{|\mathbf{n}|} = \frac{\nabla c}{|\nabla c|}. \quad (23)$$

The simplest SPH expression of ∇c is found from Eq. (6)

$$\mathbf{n}_a = \sum_b c_b \nabla_a W_{ab}(h) \Omega_b. \quad (24)$$

However, more accurate solutions for the normal vectors are obtained when the color field is smoothed by convolution with a kernel (Morris, 2000)

$$\tilde{c}_a = \sum_b c_b W_{ab} \Omega_b, \quad (25)$$

and Eq. (24) is rewritten into the symmetrical form

$$\mathbf{n}_a = \varrho_a \sum_b (\tilde{c}_b - \tilde{c}_a) \nabla_a W_{ab}(h) \Omega_b. \quad (26)$$

The curvature of the interface can be obtained with the relation

$$\kappa = -\nabla \cdot \widehat{\mathbf{n}}. \quad (27)$$

However, independently of the use of either Eq. (24) or (26), large errors of curvature can occur. Morris (2000) found that the sources of the error are the regions located far from the interface,

but still in the smoothing transition zone where \mathbf{n} is small but yet non-zero. The normalization procedure (23) can even increase the computational errors. To avoid this difficulty, we use the special criteria, proposed by Morris (2000), to determine the normal vectors that can lead to errors.

Finally, assuming $\delta_s = |\mathbf{n}|$, the surface tension can be included in the r.h.s. of the N-S equation (8) adding the term

$$\mathbf{a}_a = \frac{\sigma_a}{\rho_a} \kappa_a \mathbf{n}_a. \quad (28)$$

Interface sharpness

In the case of high density ratios between the two phases, we have found that results can suffer from a spurious fragmentation of the interface (the micro-mixing of SPH particles). A similar behavior was also reported by Colagrossi and Landrini (2003) and by Grenier et al. (2009), but these authors suggested that the problem appears only when surface tension is negligible. To prevent this and to control the interface sharpness, following Grenier et al. (2009), an additional term in the N-S equation is used and rewritten here into an multi-phase SPH variant

$$\Xi_a = \frac{\varepsilon}{m_a} \sum_{\text{if } c_b \neq c_a} \left(\left| \frac{p_a}{\Omega_a^2} \right| + \left| \frac{p_b}{\Omega_b^2} \right| \right) \nabla_a W_{ab}(h) \quad (29)$$

where ε is a suitably-chosen parameter. The role of this term is to introduce a small repulsive force between phases. A similar idea was proposed by Das and Das (2009) for the SPH simulations of submerged orifices, where a special no-penetration force $\mathbf{\Pi}_{ab}$ between particles is used

$$\mathbf{\Pi}_{ab} = \frac{\varepsilon}{m_a} \begin{cases} (P_d^6 - P_d^4) \mathbf{r}_{ab} / r_{ab}^2, & \text{if } P_d \geq 1, \\ 0, & \text{if } P_d < 1, \end{cases} \quad (30)$$

where $P_d = h/r_{ab}$. However, both Eq. (29) and Eq. (30) are dependent on the empirical constant ε that changes with the type of fluid and, even, with the flow considered. In the present work, we use Eq. (29). However, further studies to resolve this issue are necessary.

Incompressibility constraint

The most common method of implementing the incompressibility constraint is the use of a weakly compressible formulation (WCSPH). It involves the set of governing equations closed by a suitably-chosen artificial equation of state $p = p(\rho)$. Since pressure is an explicit function of ρ , the density gradient exerts an influence on the particle motion. The commonly used equation of state has the form

$$p = \frac{c^2 \rho_0}{\gamma} \left[\left(\frac{\rho}{\rho_0} \right)^\gamma - 1 \right], \quad (31)$$

where ρ_0 is the initial (reference) density. The sound speed c and a parameter γ are suitably chosen to reduce the density fluctuations down to 1%. In the present work we set $\gamma = 7$ and c at the level at least 10 times higher than the maximal fluid velocity.

We note that an alternative formulation (ISPH-GPS and ISPH-PPS) exists where the incompressibility constraint is explicitly enforced through the pressure correction procedure (Cummins

and Rudman, 1999) to satisfy $\nabla \cdot \mathbf{u} = 0$ (projection method). Additionally, another pressure correction may be used to enforce a constant fluid density, which is quite important and often overlooked (Pozorski and Wawrenczuk, 2002). These issues with further developments are amply addressed in (Szewc et al., 2012a).

NUMERICAL RESULTS

The Rayleigh-Taylor instability

The Rayleigh-Taylor instability is the test that requires an accurate modelling of the interface between two fluids. It involves two fluids closed in rectangular domain. Initially, the phases are separated by the interface located at $y = 1 - 0.15 \sin(2\pi x)$. The lower component has density $\varrho = 1$, while the upper one $\varrho = 1.8$. Since the system occurs under gravity $\mathbf{g} = [0.0, -1.0]$ and the upper phase is heavier, an instability arises and the vorticity is generated. For this flow, the Reynolds number is defined as

$$Re = \frac{\sqrt{\left(\frac{H}{2}\right)^{3/2} g}}{\nu} = 420, \quad (32)$$

where $H = 2$ is the height of the domain and kinematic viscosity $\nu = 1/420$.

The simulations were performed for two spatial resolutions: 60×120 and 120×240 particles homogeneously distributed in the domain. Figure 1 presents the SPH simulations compared to the Level-Set reference solutions obtained by Grenier et al. (2009). The spatial resolution of the Level-Set simulation is very high: 312×624 cells. Even for small number of particles in domain (60×120) the SPH results and the precise Level-Set computations exhibit similar interface shapes. Increasing the number of particles in the SPH case (see 120×240 particles calculations) the interface shape becomes much sharper. For more details, see Szewc et al. (2011).

In the considered case of the Rayleigh-Taylor instability, the obtained results suffer from a spurious fragmentation of the interface (the micro-mixing), cf. Fig. 2(left). To prevent this and to control the interface sharpness, an additional term (29) can be used. The comparison of the particle distributions near the interface using the SPH approach with and without the sharpness correction procedure is presented in Fig. 2.

Air bubble rising in water (2-D, no surface tension)

The simulations of air bubbles moving in a liquid are important because such situations (only seemingly simple) commonly occur in two-phase flows with interfaces. For testing purposes, the gas-liquid systems containing, initially placed, a bubble of radius $R = 1$, located close to the bottom of the domain (and subject to buoyancy). The density ratio of liquid (L) and gas (G) phases was equal $\varrho_L/\varrho_G = 1000$, while the kinematic viscosity ratio was $\nu_L/\nu_G = 1/128$. In this case, the Reynolds number can be defined as

$$Re = \frac{\sqrt{(2R)^3 g}}{\nu_L}, \quad (33)$$

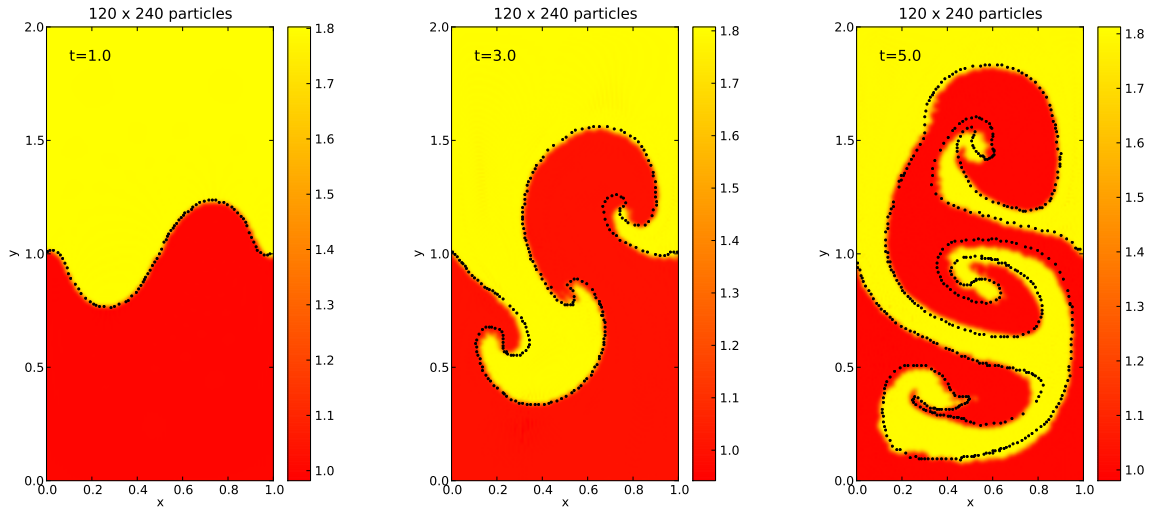


Figure 1: The density field at $t = 1, 3, 5$ for the Rayleigh-Taylor instability using 120×240 particles. The black points denotes the interface position obtained with the Level-Set formulation (312×624 cells) Grenier et al. (2009). Simulation was performed utilizing the SPH approach with $Re = 420$. Figures from the paper (Szewc et al., 2011).

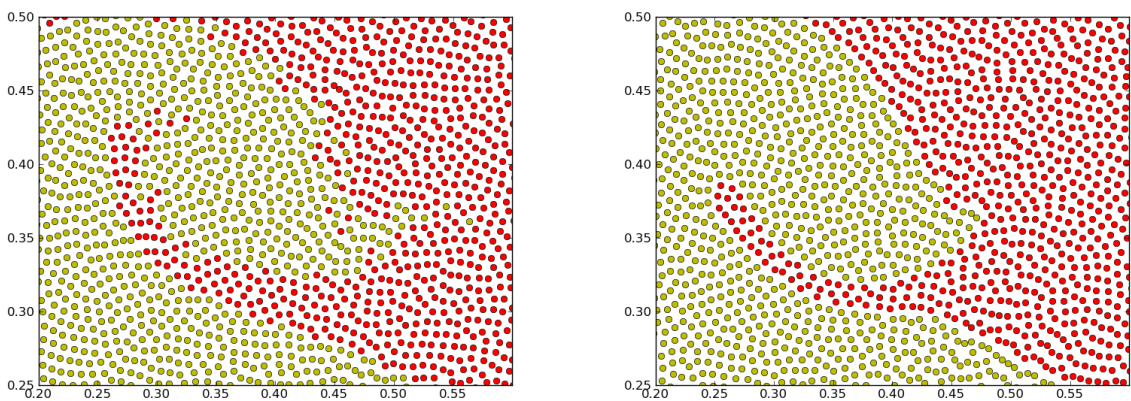


Figure 2: The particle distributions near the interface; (left) without, (right) with the sharpness correction procedure.

while the influence of the surface-tension can be described by the Eötvös number

$$Eö = \frac{4\rho_L g R^2}{\sigma}. \quad (34)$$

The SPH simulations were performed with Eq. (29) to control the sharpness of the interface. Particles were initially regularly distributed on 120×200 lattice. The gas inside bubble was treated as compressible ($\gamma = 1.4$). Figure 3 presents an evolution of air bubble rising in water for $Re = 1000$ and no surface tension compared to the data obtained using the Level-Set method by Sussman et al. (1994). The comparison shows that both approaches yield similar shapes of the interface. Initially circular bubble deforms to take horseshoe shape and finally splits into parts. Similar comparisons were performed by Colagrossi and Landrini (2003) and Grenier et al. (2009). All the results are in very good accordance. A broader selection of rising regimes is discussed in Szewc et al. (2012b).

Heat conduction in slabs (heat transfer validation)

The simplest configuration that allows us to assess the SPH formulation of heat transfer is a finite, two-dimensional rectangular (1×1) slab where two opposite sides (left and right) have fixed temperatures T^l and T^r , respectively, and the other two sides are adiabatic. From the mathematical point of view this is a one-dimensional test problem. For the testing purposes, two qualitatively different cases are considered here: homogeneous and inhomogeneous (in the sense of material properties). In the homogeneous case, the material properties are $c_p = 1$, $k = 1$ and $\rho = 1000$. In the inhomogeneous case, the slab is divided at $x = 0.5$ (along y axis) into two parts (left and right) with different material properties: $c_v^l = 1, k^l = 1, \rho^l = 1000, c_v^r = 1.5, k^r = 3, \rho^r = 2000$. For both cases considered here $T^l = 0$ and $T^r = 1$. The initial temperature distribution in the slab is presented in Figs. 4(left) and Figs. 5(left). For both cases, the approximate analytical solution, obtained for infinite slabs, is (Carslaw and Jaeger, 1965)

$$T = T^l + T^c \begin{cases} \text{Erfc}\left(\frac{0.5-x}{2\sqrt{a^l t}}\right) & \text{if } x < 0.5 \\ 1 + \frac{k^l}{k^r} \sqrt{\frac{a^r}{a^l}} \text{Erf}\left(\frac{x-0.5}{2\sqrt{a^r t}}\right) & \text{if } x > 0.5 \end{cases} \quad (35)$$

where

$$T^c = \frac{k^r / \sqrt{a^r}}{k^r / \sqrt{a^r} + k^l / \sqrt{a^l}} (T^r - T^l), \quad (36)$$

and $a = k/\rho c_p$ denotes the thermal diffusivity. The temperature profiles of the SPH computations and the analytical solutions at $t = 10$ (transient solution) are presented in Figs. 4(right) and Figs. 5(right). For both cases the comparison of SPH with the analytical solution shows a very good accordance.

Differentially heated square cavity

A differentially heated square cavity is presented in Fig. 6. The left and right boundaries are isothermal, maintained respectively at T_c (cold) and T_h (hot); both horizontal walls are adiabatic. The governing equations in a non-dimensional form are given as

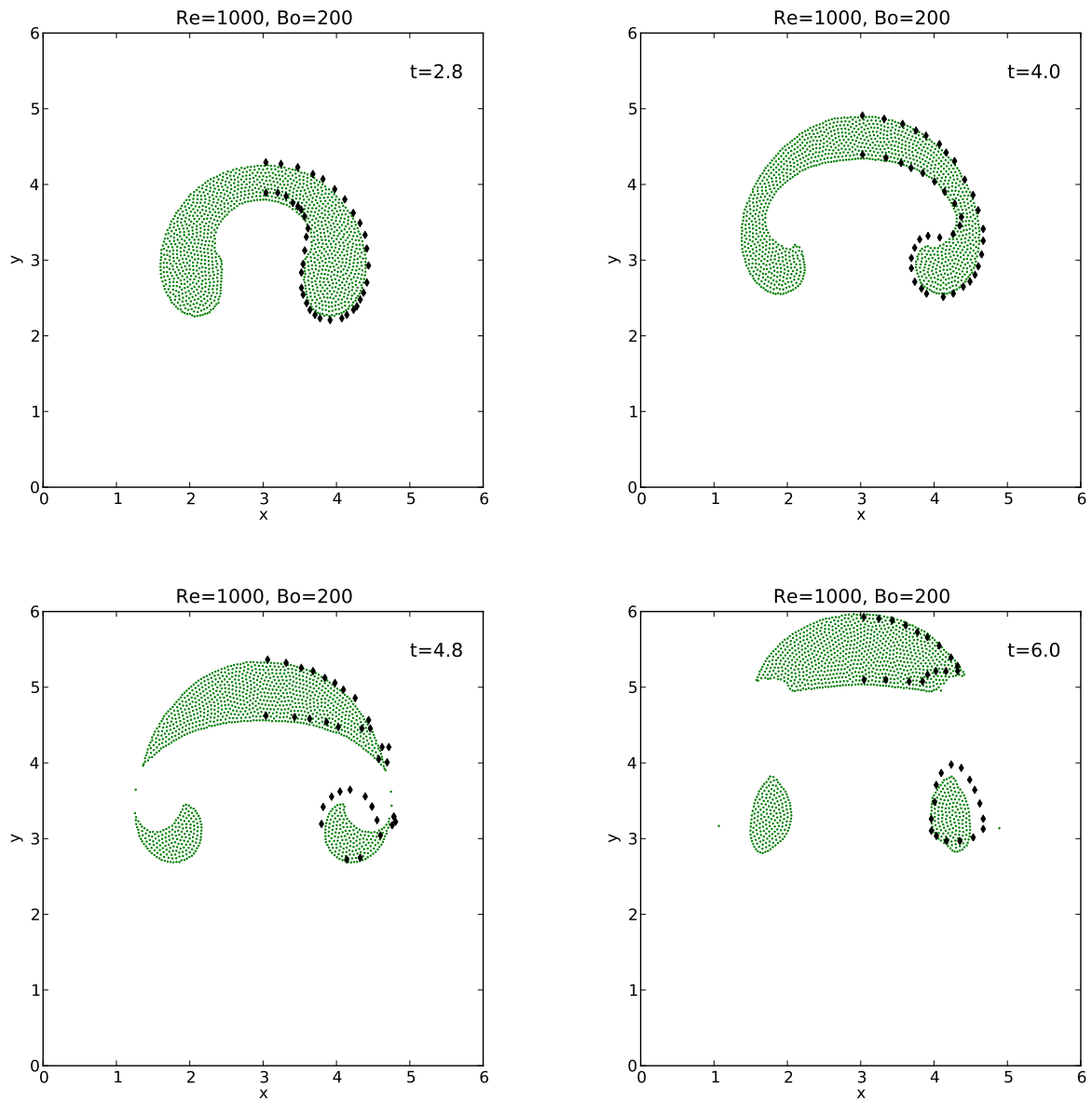


Figure 3: Evolution of air bubble rising in water with high Reynolds number (still laminar) and no surface-tension ($Re = 1000$, density 1000/1); the green points denote SPH solution computed with the Hu and Adams formulation and the interface sharpness control procedure; the black diamonds represent the interface obtained with the Level-Set formulation by Sussman et al. (1994) ($E\ddot{o} = 200$ - negligible surface-tension).

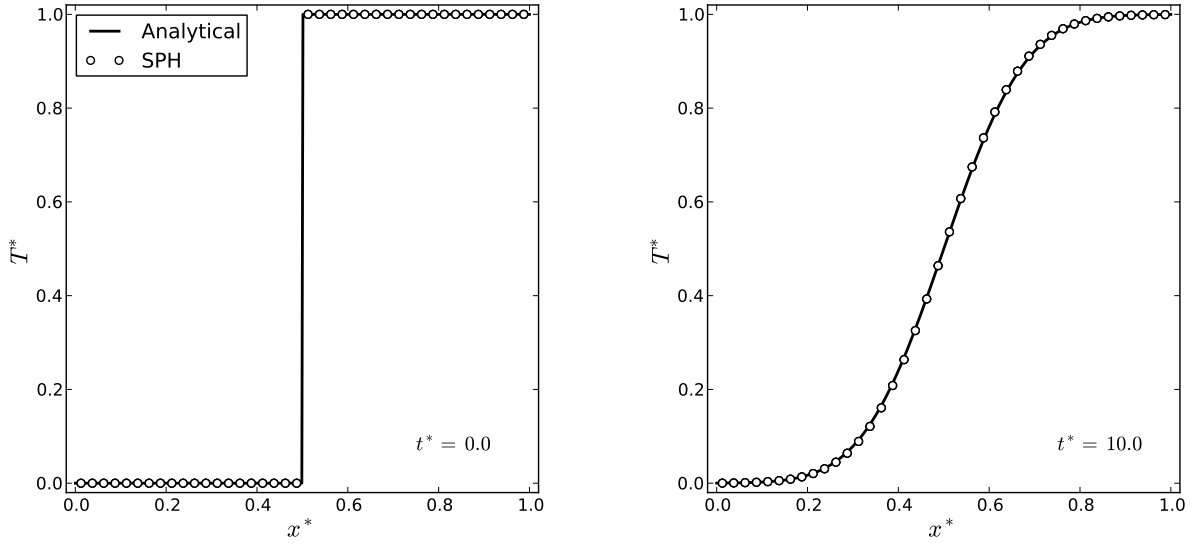


Figure 4: The SPH computations of temperature profile (dots) across the homogeneous slab ($c_v^l = c_v^r = 1, k^l = k^r = 1, \varrho^l = \varrho^r = 1000$) for: (left) initial state $t = 0$ and (right) $t = 10$; the analytical solutions (Carslaw and Jaeger, 1965) are given by the solid line; all the results expressed in the dimensionless form.

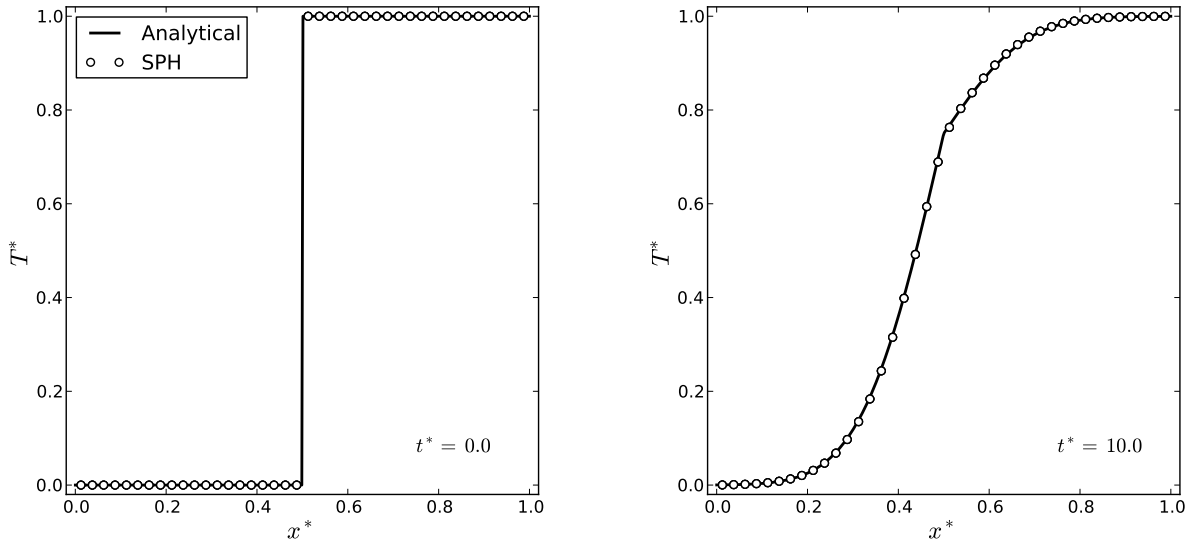


Figure 5: The temperature SPH computations (dots) across the inhomogeneous slab ($c_v^l = 1, k^l = 1, \varrho^l = 1000, c_v^r = 1.5, k^r = 3, \varrho^r = 2000$) for: (left) initial state $t = 0$ and (right) $t = 10$; the analytical solutions (Carslaw and Jaeger, 1965) are given by the solid line; all the results expressed in the dimensionless form.

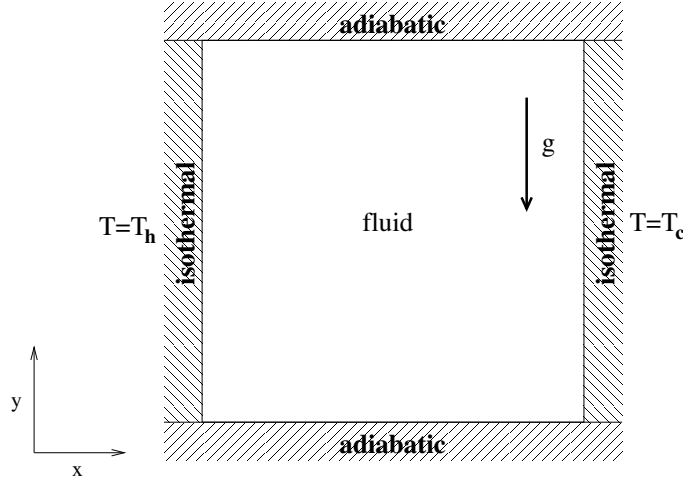


Figure 6: A scheme of a differentially heated square cavity. Figure from the paper (Szewc et al., 2011).

$$\frac{\partial u_i^*}{\partial x_i^*} = 0, \quad (37)$$

$$\frac{\partial u_i^*}{\partial t^*} + u_j^* \frac{\partial u_i^*}{\partial x_j^*} = -\frac{\partial p^*}{\partial x_i^*} + Pr \frac{\partial^2 u_i^*}{\partial x_j^* \partial x_j^*} + RaPrT^* \delta_{i2} \quad (38)$$

$$\frac{\partial T^*}{\partial t^*} + \frac{\partial u_j^* T^*}{\partial x_j^*} = \frac{\partial^2 T^*}{\partial x_j^* \partial x_j^*}, \quad (39)$$

and

$$x_i^* = \frac{x_i}{L}, u_i^* = \frac{u_i L}{a}, p^* = \frac{pL^2}{\rho a^2}, t^* = \frac{tL^2}{a}, T^* = \frac{T - T_c}{T_h - T_c}. \quad (40)$$

where L is the size of the cavity, while the Rayleigh number is defined with $\mathbb{L} = L$ and $\Theta = T_h - T_c$.

In order to validate SPH approach, natural convection in the differentially-heated cavity is studied at 10^5 with $Pr = 0.71$. Simulations were performed using 3600 particles in the domain. Figure 7 shows the velocity and temperature fields obtained by SPH using the Boussinesq approximation. The local Nusselt number Nu , which describes the ratio of convective to conductive heat transfer across the wall, is defined as

$$Nu(y) = \left. \frac{\partial T^*}{\partial x^*} \right|_{y \in wall}. \quad (41)$$

Figure 8 shows SPH computations of the local Nusselt number distribution along the cold wall obtained both with the Boussinesq approximation and with the proposed approach. Reference data were computed by Wan et al. (2001) using DCS method. The simulated local Nusselt number distributions look very realistic. For more results, also including a more general non-Boussinesq formulation proposed by the author, see (Szewc et al., 2011).

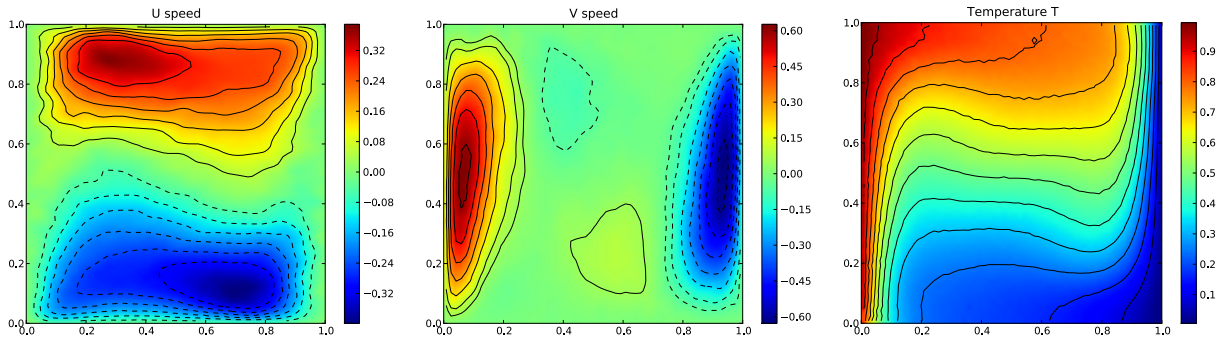


Figure 7: Horizontal velocity (left plots), vertical velocity (middle plots) and temperature field (right plots) for horizontally-heated square cavity at $Ra = 10^5$ and $Pr = 0.71$ (steady-state solution). Figures from the paper (Szewc et al., 2011).

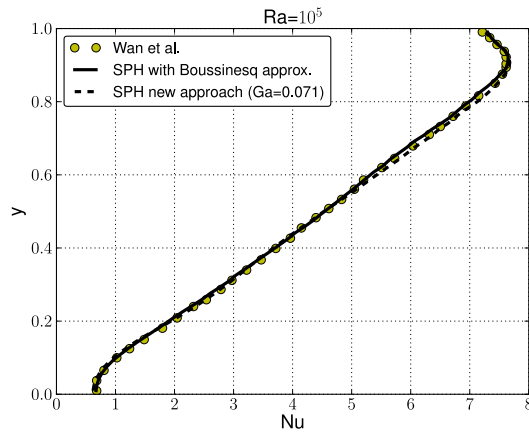


Figure 8: The local Nusselt number distribution along the cold wall for $Ra = 10^5$ (right). Reference data obtained by Wan et al. (2001) using DSC technique. Figure from the paper (Szewc et al., 2011).

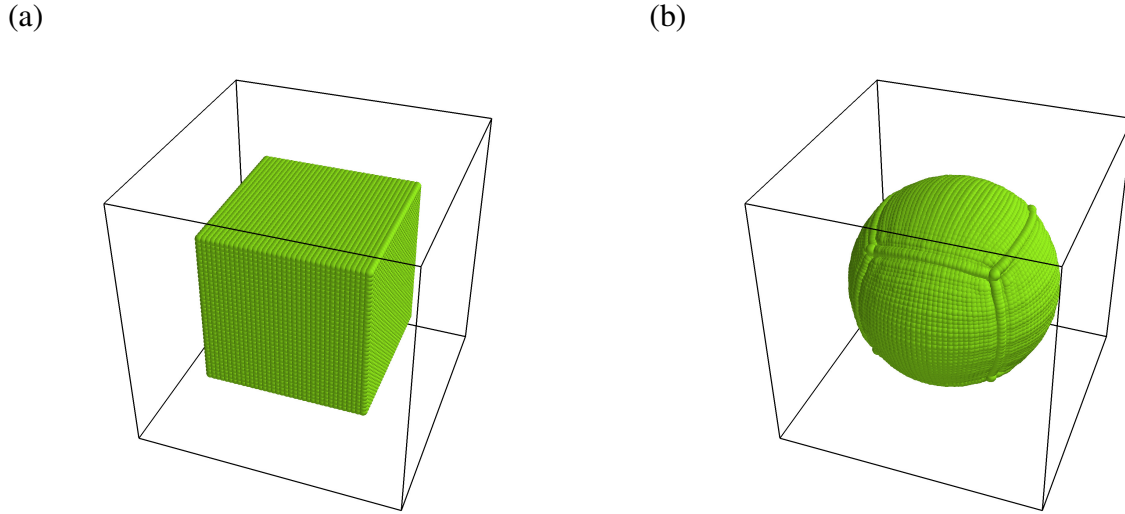


Figure 9: Particle distribution (only the inner phase) of the cube-to-sphere deformation test: (a) the initial state, (b) the steady-state solution obtained with the CSF method (Brackbill et al., 1992; Morris, 2000). Figure from the paper (Szewc et al., 2012a).

Cube-to-sphere droplet deformation (surface tension validation)

The simplest three-dimensional flow case governed by surface-tension phenomena is the cube-to-sphere droplet deformation. It involves a cubical box of fluid with the edges of length L containing the inner phase of centered cubical volume of another fluid of the edges $a = 0.6L$.

The density of both phases is ϱ and the viscosity coefficient ν . The influence of surface tension is described by the Weber number, $We = \varrho au^2/\sigma$, whereas the capillary number, $Ca = \varrho \nu u/\sigma$, accounts also for viscosity. Here, we chose $Ca^2/We = \nu^2 \varrho/a\sigma = 2/30$. The capillary number, based on the maximum velocity in domain, is about 0.45. Since the surface tension is present, the initially cubic volume of the inner phase ultimately takes the spherical shape, cf. Fig. 9. From the Laplace law the pressure inside the formed droplet must be higher than in the surrounding fluid and should undergo a jump across the interface

$$\Delta p = \sqrt[3]{\frac{4\pi}{3} \frac{2\sigma}{a}}. \quad (42)$$

The simulation was performed with $N = 216\,000$ particles ($60 \times 60 \times 60$), $h/\Delta r = 2$ and the Wendland kernel using different incompressibility variants (WCSPH, ISPH-GPS, ISPH-PPS, and ISPH-PPS with density correction procedure), for details cf. (Szewc et al., 2012a). The steady-state pressure profiles are presented in Fig. 10. For the incompressibility variant, which we use in the present work (WCSPH), the SPH solution is in a good agreement with the analytical formulae.

Air bubble rising in water (3D)

To validate the SPH approach, we compared the results to the experimental data of Bhaga and Weber (1981). For all the considered cases, the regular domain filled with liquid and containing a

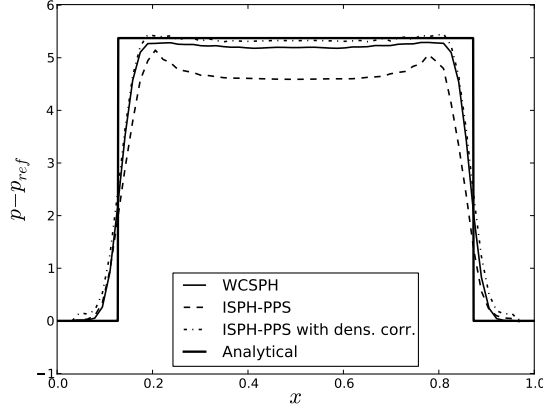


Figure 10: The cube-to-sphere deformation test: the computed pressure profiles at the steady-state solution (against the analytical solution). Figure from the paper (Szewc et al., 2012a).

single bubble of the initial diameter D is considered. The domain is taken as sufficiently large in each direction ($L > 5D$, where L is the domain size) so that the wall confinement effects can be neglected. The results are presented in terms of the following dimensionless numbers

$$\text{Reynolds number, } Re = \frac{\rho_L D U_T}{\mu_L}, \quad (43)$$

$$\text{Eötvös number, } E\ddot{o} = \frac{g D^2 \rho_L}{\sigma}, \quad (44)$$

$$\text{Morton number, } Mo = \frac{g \mu_L^4}{\rho_L \sigma^3}, \quad (45)$$

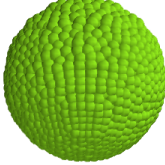
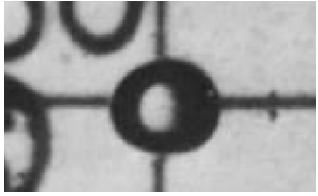
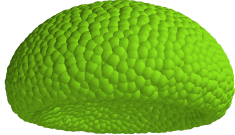
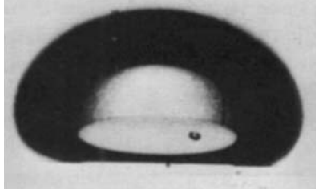
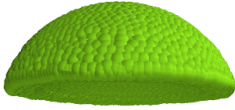
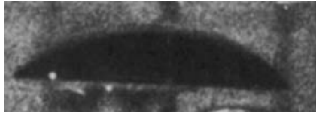
where U_T is terminal rise velocity, while ρ , μ , σ and g are, respectively, the density, dynamic viscosity, surface tension coefficient and the acceleration of gravitation. Subscripts L and G denote respectively liquid and gas phase. It is important to note that the full information about the properties of fluid (which have impact on the dynamics) is described by the set of two dimensionless numbers: $E\ddot{o}$ and Mo . The gas-liquid density and viscosity ratio are respectively $\rho_L/\rho_G = 1000$ and $\mu_L/\mu_G = 100$. The results of 3-D SPH simulations are summarized in Table 1 which provides the comparison of current simulations with the reference data. The presented comparison shows that the SPH approach is in a very good qualitative accordance with the reference data.

For the Morton numbers greater than $Mo = 4 \cdot 10^{-3}$ both the drag coefficient C_D and a bubble shape depend on the Reynolds number only; in this regime, Bhaga and Weber (1981) proposed the experimental correlation in the form

$$C_D = \left(2.67^{0.9} + (16/Re)^{0.9} \right)^{1/0.9}. \quad (46)$$

Figure 11 presents obtained SPH results compared to correlation (46). Presented SPH solutions show very good accordance with the experimental results. A comprehensive comparison with other numerical approaches (Front-Tracking, Lattice Boltzmann) is reported in Szewc et al. (2012b).

Table 1: Comparison of 3D SPH simulation results with experimental data by Bhaga and Weber (1981).

Case	SPH	Experiment
$Eö = 17.7 \quad Mo = 711$		
$Eö = 243 \quad Mo = 266$		
$Eö = 115 \quad Mo = 4.63 \cdot 10^{-3}$		

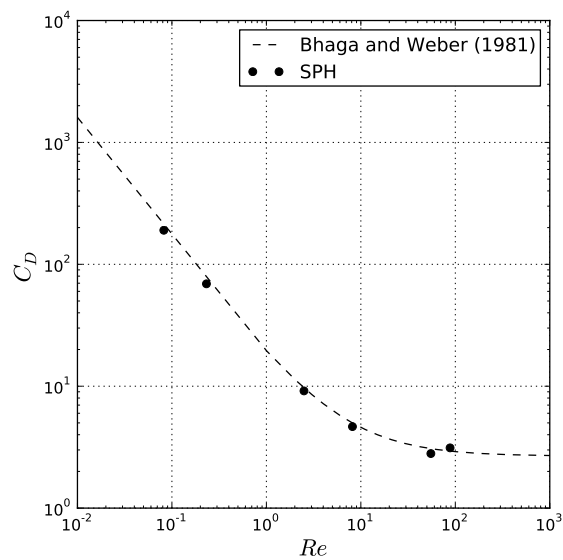


Figure 11: Drag coefficient - Reynolds number relationship comparison between the SPH solution and the experimental correlation by Bhaga and Weber (1981).

PHASE CHANGE

A numerical solution of the phase-change problem involves the modelling of many coupled elements like the momentum and energy equations, the latent heat and interphase mass transfer, the surface tension forces, discontinuities of material properties, and finally the interface shape tracking. In the case of Eulerian CFD approaches, some of the above are treated with no major difficulty, yet some others are a little bit tricky. The examples are the computation of the position of the interface in VOF (Hirt and Nichols, 1981), MAC (Harlow and Welch, 1965; McKee et al., 2008) and the Level Set (Sussman et al., 1994) approaches or, in general, the one fluid approximation. However, these methods have proven to be efficient and sufficiently accurate for many cases of phase change phenomena (Juric and Tryggvason, 1998; Jeon et al., 2009; Kunkelmann and Stephan, 2010; Tryggvason et al., 2005).

Due to the Lagrangian formalism of Smoothed Particles Hydrodynamics, the problems with taking into account the discontinuity of material properties or with the interface tracking disappear using this approach. However, this does not mean that SPH is an obvious choice for computing phase change phenomena.

The first implementation of the phase change in SPH was proposed by Cleary et al. (2006); Cleary (2010) to simulate the solidification of liquid metals, cf. next subsection. Using this approach, the authors obtained very accurate simulations of casting processes including shrinkage of cooling metal, tracking of oxide formation, prediction of feeding, solidification front dynamics and prediction of the residual pressure distribution of solidified metal.

However, various complications appear when the liquid-vapor phase change is considered. Analysing the process of boiling macroscopically, when the temperature of the liquid near the interface is equal to (or higher than) the saturation temperature T_{sat} , the phase change and, consequently, the interphase mass transfer occurs. The main problem is a huge difference of the densities between phases. Due to this inconvenience the recolouring procedure of particles can not be considered. Namely, with the discretised (or particle) representation of the continuum in SPH formalism, it is convenient to attribute the same masses or volumes to all particles. As discussed earlier, particles representing different phases are tagged with different integer identifiers (“colours”). For a particle located next to the interface, the change of phase is, at a first (naive) sight, equivalent to changing its color during the single time step or in an integer number of time steps (determined by the local heat flux conditions). But at the same time, the particle properties may drastically change, involving numerical instabilities. In particular, in typical conditions of boiling or condensation the density may change by a factor as large as $O(10^3)$.

Yet, the problem is not only the numerical one; even from the physical point of view there remain still unresolved issues such as the proper boundary condition for temperature at the interface (Juric and Tryggvason, 1998) or the liquid-bubble heat transfer mechanisms (Kim, 2009). So, apart from fluid-dynamical issues, also the non-equilibrium thermodynamics becomes involved in the picture.

The first SPH simulations of evaporation, taking into account only the van der Waals model of fluid, based on the model developed by Tartakovsky and Meakin (2005); Tartakovsky et al. (2009), were performed by Charles and Daivis (2009). However, that application was limited only to the mesoscopic scale flows.

Our first ideas and sketches for implementation of the liquid-vapour phase change in the macroscopic scale are presented below. They are subject to further discussions and subsequent modifications.

Melting, freezing

The simulations of the solidification phenomena ("freezing") are of importance for many industrial and environmental problems. Examples include the die casting processes or the formation of ice on rivers. From the numerical point of view, due to rather small density changes, this is the simplest case of the phase change phenomena.

To simulate such processes, Cleary (2010) proposed the WCSPH approach with the set of governing equations composed of the Navier-Stokes equation

$$\frac{d\mathbf{u}_a}{dt} = - \sum_b m_b \left[\left(\frac{p_a}{\rho_a^2} + \frac{p_b}{\rho_b^2} \right) - \frac{4}{\rho_a \rho_b} \frac{\mu_a \mu_b}{\mu_a + \mu_b} \frac{\mathbf{u}_{ab} \cdot \mathbf{r}_{ab}}{\mathbf{r}_{ab}^2 + \eta^2} \right] \nabla_a W_{ab}(h), \quad (47)$$

the continuity equation

$$\frac{d\rho_a}{dt} = \sum_b m_b \mathbf{u}_{ab} \cdot \nabla_a W_{ab}(h), \quad (48)$$

and the energy equation, written in terms of enthalpy (which is generally preferred for flows with phase changes)

$$\frac{dH_a}{dt} = \sum_b \frac{4m_b}{\rho_a \rho_b} \frac{k_a k_b}{k_a + k_b} \frac{T_{ab} \mathbf{r}_{ab}}{\mathbf{r}_{ab}^2 + \eta^2} \cdot \nabla_a W_{ab}(h). \quad (49)$$

The enthalpy per unit mass H is defined as

$$H = \int_0^T c_p(\Theta) d\Theta + L[1 - f_s(T)], \quad (50)$$

where L is the latent heat, and $f_s(T)$ is the local volume fraction of solid at temperature T . For the solidification modelling, the authors consider two different approaches. The first one involves a viscosity dependency with temperature. In this approach the solid phase is represented as a viscous pseudo-fluid. However, this does not allow to preserve stresses in the solidified metal. In the second approach (stress-preserving), when the temperature of fluid particle is lower than the solidus temperature and this particle has more than one neighbours representing the solid phase, then the N-S equation changes to another equation more suitable for solids (e.g., stopping a particle and freezing it in occupied place).

Boiling, condensing

The ability of fluids to store and then transfer large amounts of energy in the form of the latent heat when boiling or condensation occurs is the key property exploited for energy management in many industrial applications. Among other processes and devices, the liquid-vapour phase change is crucial for heat exchangers in fossil power plants or in the primary circuits of nuclear reactors

where huge amounts of energy have to be extracted from the core as efficiently as possible. In the following, we will focus on boiling; yet, the modelling and numerical difficulties involved with condensation are similar.

When the phase change occurs in a liquid coolant (nucleate boiling), the energy is stored in the form of latent heat. Moreover, bubble formation may induce a considerable local velocity of the liquid layer on the heated surface. Both factors imply a substantial increase of heat transfer. However, the practical use of boiling is limited by the condition called the critical heat flux or boiling crisis. It occurs when the boiling regime changes, with the increase of wall heat flux, from the subcooled (nucleate) boiling, through the so-called departure from nucleate boiling (DNB), the film boiling, up to the extreme situations when the evolution of vapour prevents the liquid from approaching the surface and the heat transfer suddenly decreases. Further increase of the wall heat flux causes that a continuous layer of vapour approaches the heating wall so the surface is isolated from the liquid. Then, all the heat transfer occurs only due to the radiation and convection in gaseous phase. The prevention from DNB and, in consequence, from the overheating (“burnout”) of the heating surface is one of the most important issues in many engineering problems where heat production and conversion are crucial.

As mentioned in the Introduction, the main problem in the implementation of phase change in the SPH approach is a huge density difference between the phases and, therefore, the recolouring of particles (obviously) can not be used to reproduce the mass interphase transport. Moreover, since in the SPH the particles represent the volume elements of the fluids, the splitting and joining of particles procedure seems to be unrealistic. This is because of the fact that one particle of liquid should represent one thousand particles of vapour, say, while solutions based on fractional particles do not come into play.

However, a huge difference between densities of phases suggests another, simple solution. After the nucleation, vapour bubbles change their size due to the interphase mass flow. When a bubble grows, the number of SPH particles representing the gaseous phase should increase. Yet, due to the density difference, the change of the liquid volume can be considered as negligible. Therefore, the liquid phase may be approximated as an infinite reservoir of the vapour. This is adequate for the test problem of the bubble growth due to evaporation in the bulk of liquid. Of course, with this approach the mass of the liquid phase does not change, therefore, the processes such as film boiling or total evaporation, cf. Juric and Tryggvason (1998), can not be considered this way.

However, such an approach implies two problems that must be solved. The first one is the computation of the mass transfer rate \dot{m} across the interface. The good solution, used in many Eulerian implementations of boiling (Jeon et al., 2009; Kunkelmann and Stephan, 2010), is

$$\dot{m} = \frac{\dot{q}}{L}, \quad (51)$$

where \dot{q} denotes the interphase heat transfer rate, and L is the enthalpy of vaporization. Assuming that the heat conductivity on the interface is equal to heat conductivity in liquid, we can write the approximate relation

$$\dot{m} = \frac{k(T_{\text{sat}} - T_L)S}{L\phi}, \quad (52)$$

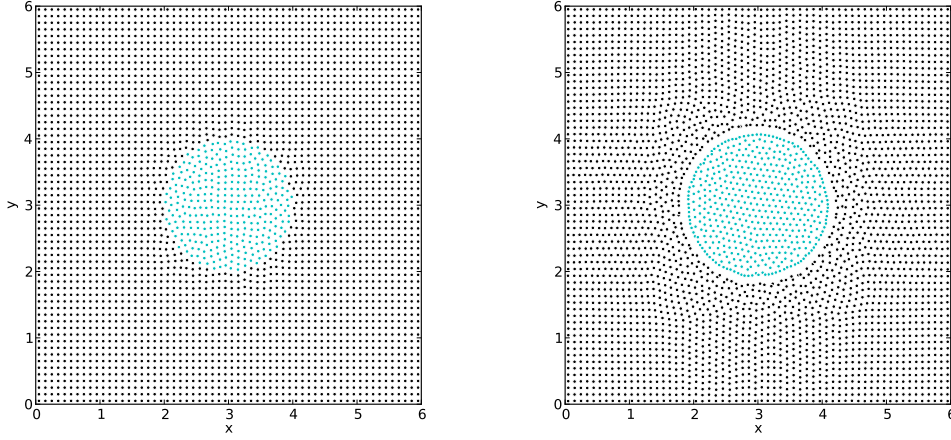


Figure 12: Distributions of the SPH particles in domain for the air bubble submerged in water with no gravity force; the simulations performed without (left) and with (right) the particle pushing phenomena.

where ϕ is the mean distance to the interface

$$\phi = \sum_{b, \text{ if } c_b \neq c_a} \frac{m_b}{\rho_b} |\mathbf{r}_b| W_{ab}(h), \quad (53)$$

while S is the area of the liquid-vapour interface which represents the particle.

The second problem is the computation of the position where the newly generated vapour particle has to appear. The very first idea of its solution is presented below.

Particle pushing algorithm

Here, we propose a simple idea for locating (“pushing”) new particles, originated in one phase, in the other phase. Since we treat the liquid as the infinite reservoir of the gaseous phase, only pushing the particles into the vapour phase subdomain is considered.

For each liquid particle placed near the interface, as measured by the smoothed value of color function ($0.4 < \tilde{c} < 0.6$), if the condition $\dot{q} > m_G$, where m_G is the mass of vapour particle, then the particle of gaseous phase is put into the position located at distance h from the particle in the direction normal to the interface.

Fig. 12 presents a distribution of the SPH particles in the domain for the air bubble of density $\rho_G = 0.001$ submerged in the liquid of density $\rho_L = 1$. The other material parameters and initial distributions are as in the case of air bubble rising in water. The Eötvös number is equal to 25. But, in this test, the gravity is turned off. The simulations were performed without (left) and with (right) the particle pushing procedure. Comparing the results, it is easy to show that some deficiency of particles appears near the interface when particle pushing is switched on. The possible reason is that the short-range repulsive force is applied on the interface to assure its sharpness. However, generally, the method seems to be useful.

In cases when the liquid phase can no longer be treated as the infinite reservoir of vapour (basically, in finite-size systems), an imaginable solution may be the addition of new vapour particles

(all of the same mass for simplicity) at time steps when the locally accumulated latent heat will trigger the generation of one such particle, at the cost of a (minor) part of the liquid particle mass next to the interface. The mass of all vapour particles is predetermined to respect the assumed spatial resolution of the growing bubbles. The location of the new vapour particle will be chosen so as to keep constant the moment of the pair (no external force effect). Then, for the sake of computational efficiency, a procedure of liquid particle management may occasionally be applied: fusion, when a prescribed mass fraction of the liquid particle underwent evaporation; alternatively, mass renormalisation or remeshing of the liquid particles.

Summary

In the present work, we discussed the usefulness of the SPH approach for modeling multi-phase flows, in particular those governed by buoyancy. The study has been supported by numerically demanding two- and three-dimensional cases: the Rayleigh-Taylor & Rayleigh-Bernard instabilities, an air bubble rising in water, and also, heat conduction in slab and the cube-to-sphere droplet deformation. Obtained results were compared to the available data from the literature (both analytical and numerical). Comparisons with other numerical methods emphasize the interest of the present method. One weakness of the present formulation of the SPH approach, namely the spurious fragmentation of the interface (micro-mixing), has been also discussed but further studies are necessary to resolve this issue. Since this work is an intermediate step in a complete project which aims at simulating boiling phenomena with the SPH approach, a part of the paper has been devoted to the potential use of the SPH method to simulate phase change phenomena. Since, at present, the SPH variants based on fractional particles are not known, a large difficulty in SPH is the liquid-vapour mass transfer. As an alternative, the method of creating new vapour particles has been proposed. Since we treat the liquid as the infinite reservoir of the gaseous phase, only pushing the particles into the vapour phase subdomain is considered here. These proposals are currently evaluated.

Acknowledgment

One of the authors (KS) is indebted to the Polish Science Foundation (FNP) for a research scholarship START 2012.

References

- Bhaga, D., Weber M.E., (1981): Bubbles in viscous liquids: shapes, wakes and velocities, *J. Fluid Mech.*, Vol. 105, pp. 61-85.
- Brackbill, J.U., Kothe, D.B., Zemach, C., (1992): A continuum method for modelling surface tension, *J. Comput. Phys.*, Vol. 100, pp. 335-354.
- Brennen, C.E., (2005): *Fundamentals of Multiphase Flow*. Cambridge Univ. Press, Cambridge.
- Carslaw, H.S., Jaeger, J.C., (1965): *Conduction of Heat in Solids*, Oxford University Press, London.
- Charles, A., Davis, P., (2009): Smooth Particle Hydrodynamics for Vapour Liquid Coexistence, 18th World IMACS-MODSIM Congress, Cairns, Australia.
- Cleary, P.W., Monaghan, J.J., (1999): Conduction modelling using smoothed particle hydrodynamics, *J. Comput. Phys.*, Vol. 148, pp. 227-264.

- Cleary, P.W., Ha, J., Prakash, M., Nguyen, T., (2006): 3D SPH flow predictions and validation for high pressure die casting of automotive components, *Applied Mathematical Modelling*, Vol. 30, pp. 1406-1427.
- Cleary, P.W., (2010): Extension of SPH to predict feeding, freezing and defect creation in low pressure die casting, *Applied Mathematical Modelling*, Vol. 34, pp. 3189-3201.
- Colagrossi, A., Landrini, M., (2003): Numerical simulation of interfacial flows by smoothed particle hydrodynamics, *J. Comput. Phys.*, Vol. 191, pp. 448-475.
- Cummins, S.J., Rudman M., (1999): An SPH projection method, *J. Comput. Phys.*, Vol. 152, pp. 584-607.
- Das, A.K., Das, P.K., (2009): Bubble evolution through submerged orifice using smoothed particle hydrodynamics, Basic formulation and model validation, *Chem. Eng. Sci.*, Vol. 64, pp. 2281-2290.
- Gingold, R.A., Monaghan J.J., (1977): Smoothed Particle Hydrodynamics: Theory and application to non-spherical stars, *Mon. Not. R. Astron. Soc.*, Vol. 181, pp. 375-389.
- Grenier, N., Antuono, M., Colagrossi, A., Le Touzé, D., Alessandrini, B., (2009): An Hamiltonian interface SPH formulation for multi-fluid and free surface flows, *J. Comput. Phys.*, Vol. 228, pp. 8380-8393.
- Harlow, F., Welch, J.E., (1957): Numerical calculation of time-dependent viscous incompressible flow of fluid with a free surface, *Physics of Fluids*, 8, pp. 2182-2189.
- Hirt, C.W., Nichols, B.D., (1981): Volume of fluid (VOF) method for the dynamics of free boundaries, *Journal of Computational Physics*, Vol. 39, pp. 201-225.
- Hu, X.Y., Adams, N.A., (2006): A multi-phase SPH method for macroscopic and mesoscopic flows, *J. Comput. Phys.*, Vol. 213, pp. 844-861.
- Jeon, S.-S., Kim, S.-J., Park, G.-C., (2009): CFD simulation of condensing vapor bubble using VOF model, *World Academy of Science, Engineering and Technology*, Vol. 60, pp. 209-215.
- Juric, D., Tryggvason, G., (1998): Computations of boiling flows, *International Journal of Multiphase Flow*, Vol. 24, pp. 387-410.
- Kim, J., (2009): Review of nucleate pool boiling bubble heat transfer mechanisms, *International Journal of Multiphase Flow*, Vol. 35, pp. 1067-1076.
- Kunkelmann, Ch., Stephan, P., (2010): Numerical simulation of the transient heat transfer during nucleate boiling of refrigerant HFE-7100, *International Journal of Refrigeration*, Vol. 33, pp. 1221-1228.
- Lafaurie, B., Nardone, C., Scardovelli, R., Zaleski, S., Zanetti, G., (1994): Modelling merging and fragmentation in multiphase flows with Surfer, *J. Comput. Phys.*, Vol. 113, pp. 134-147.
- Lucy, L.B., (1977): A numerical approach to the testing of the fission hypothesis, *Astron. J.*, Vol. 82, pp. 1013-1024.
- McKee, S., Tomé, M.F., Ferreira, V.G., Cuminato, J.A., Castelo, A., Sousa, F.S., Mangiavacchi, N., (2008): The MAC method, *Review, Computers & Fluids*, 37, pp. 907-930.
- Monaghan, J.J., (1992): Smoothed Particle Hydrodynamics, *Ann. Rev. Astron. Astrophys.*, Vol. 30, pp. 543-574.
- Morris, J.P., Fox, P.J., Zhu, Y., (1977): Modeling Low Reynolds Number Incompressible Flows Using SPH, *Journal of Computational Physics*, Vol. 136, pp. 214-226.
- Morris, J.P., (2000): Simulating surface tension with Smoothed Particle Hydrodynamics, *Int. J. Numer. Methods Fluids*, Vol. 33, pp. 333-353.
- Nugent, S., Posch, H.A., (2000): Liquid drops and surface tension with smoothed particle applied mechanics. *Phys. Rev. E*, Vol. 62, pp. 4968-4975.
- Ohta, M., Imura, T., Yoshida, Y., Sussman, M., (2005): A computational study of the effect of initial bubble conditions on the motion of a gas bubble rising in viscous liquids, *Int. J. Multiphase Flow*, Vol. 31, pp. 223-237.
- Pianet, G., Vincent, S., Leboi, J., Caltagirone, J.P., Anderhuber, M., (2010): Simulating compressible gas bubbles with smooth volume tracking 1-Fluid method, *Int. J. Multiphase Flow*, Vol. 36, pp. 273-283.
- Pozorski, J., Wawrenczuk, A., (2002): SPH computation of incompressible viscous flows, *Journal of Theoretical and Applied Mechanics (Pol)*, Vol. 40, pp. 917-937.
- Sankaranarayanan, K., Shan, X., Kevrekidis, K., Sundaresan, I.G., (1999): Bubble flow simulations with the lattice Boltzmann method, *Chem. Sci. Eng.*, Vol. 54, pp. 4817-4823.
- Sankaranarayanan, K., Kevrekidis, K., Sundaresan, I.G., Lu, J., Tryggvason, G., (2003): A comparative study of lattice Boltzmann and front-tracking finite-difference methods for bubble simulations, *Int. J. Multiphase Flow*, Vol. 29, pp. 109-116.
- Sussman, M., Smereka, P., Osher, S.J., (1994): A level-set approach for computing solutions to incompressible two-

- phase flow, *J. Comput. Phys.*, Vol. 114, pp. 146-159.
- Swegle, J.W., Hicks, D.L., Attaway, S.W., (1995): Smoothed Particle Hydrodynamics stability analysis, *J. Comput. Phys.*, Vol. 116, pp. 123-134.
- Szewc, K., Pozorski, J., Tanière, A., (2011): Modeling of natural convection with Smoothed Particle Hydrodynamics: Non-Boussinesq formulation, *Int. J. Heat Mass Transfer*, Vol. 54, pp. 4807-4816.
- Szewc, K., Pozorski, J., Minier, J.P., (2012): Analysis of the incompressibility constraint in the SPH method, *Int. J. Numer. Methods Fluids*, in press, DOI: 10.1002/nme.4339.
- Szewc, K., Pozorski, J., Minier, J.P., (2012): Simulations of single bubbles rising through viscous liquids using Smoothed Particle Hydrodynamics, submitted to *International Journal of Multiphase Flow*.
- Takada, N., Misawa, M., Tomiyama, A., Fujiwara, S., (2000): Numerical simulation of two- and three-dimensional two-phase fluid motion by lattice Boltzmann method, *Comput. Phys. Commun.*, Vol. 129, pp. 233-246.
- Tartakovsky, A.M., Ferris, K.F., Meakin, P., (2009): Lagrangian particle model for multiphase flows, *Comput. Phys. Commun.*, Vol. 180, pp. 1874-1881.
- Tartakovsky, A., Meakin, P., (2005): Modeling of surface tension and contact angles with smoothed particle hydrodynamics, *Physical Review E*, Vol. 72.
- Tryggvason, G., Bunner, B., Esmaceli, A., Juric, D., Al-Rawahi, N., Tauber, W., Hanc, J., Nase, S., Janc, Y.-J., (2001): *J. Comput. Phys.*, Vol. 169, pp. 708-759.
- Tryggvason, G., Esmaceli, A., Al-Rawahi, N., (2005): Direct numerical simulations of flows with phase change, *Computers and Structures*, Vol. 83, pp. 445-453.
- Wan, D.C., Patnaik, S.V., Wei, G.W., (2001): A new benchmark quality solution for buoyancy-driven cavity by discrete singular convolution, *Numerical Heat Transfer, Part B*, Vol. 40, pp. 199-228.
- Wendland, H., (1995): Piecewise polynomial, positive definite and compactly supported radial functions of minimal degree, *Adv. Comput. Math.*, Vol. 4, pp. 389-396.